TRABAJO FIN DE GRADO

GRADO EN FÍSICA

FACULTAD DE CIENCIAS

TMD-based optoelectronic devices

Dispositivos optoelectrónicos basados en TMDs

Author:
Alejandro Andrés Juanes
Supervisors:
Dr. Jorge Quereda Bernabéu
Dr. Mario Amado Montero

VNiVERSiDAD D SALAMANCA

6 de julio de 2021

D. Jorge Quereda Bernabéu y D. Mario Amado Montero CERTIFICAN que el presente Trabajo de Fin de Grado, titulado TMD-based optoelectronic devices, ha sido realizado bajo su dirección por Alejandro Andrés Juanes.

Salamanca, a 6 de julio de 2021

QUEREDA BERNABEU JORGE - 50906883V

Digitally signed by QUEREDA BERNABEU JORGE - 50906883V
DN: C=ES, SERIALNUMBER=IDCES-50906883V, G=JORGE, SN=QUEREDA BERNABEU, CN=QUEREDA BERNABEU JORGE - 50906883V
Reason: I am the author of this document
Location: your signing location here
Date: 2021.07.06 19:42:16+02'00'
Foxit PDF Reader Version: 11.0.0

AMADO MONTERO MARIO - 14307293M

Firmado digitalmente por AMADO MONTERO MARIO - 14307293M
Fecha: 2021.07.06 18:54:18 +02'00'

Fdo:

D.Jorge Quereda Bernabéu.

D.Mario Amado Montero.

Abstract

Alejandro ANDRÉS JUANES

TMD-based optoelectronic devices

Recent advances in atomically thin two-dimensional materials have led to a variety of new technologies in the fields of nanoelectronics, photonics and opto-electronics. In particular, the family of Transition Metal Dichalcogenides (TMDs) is been extensively studied. The study of devices based on monolayers of these materials is of fundamental interest due to their atomically thin nature.

Some of the main challenges for 2D materials research are isolating and identifying monolayers. In this work, I describe a method to identify mono- and few-layered structures of MoS_2 through optical microscopy and its comparison to Raman spectra. Firstly, I introduce the concepts of 2D materials, TMDs and the techniques used to create a device: mechanical exfoliation and all-dry viscoelastic stamping. Then, describe the process of acquisition of images and measurement of contrasts in them; as well as what is Raman spectroscopy and how it determine the number of layers of a sample. Lastly, it is depicted a numerical model to obtain the transmittance of light and compared to the experimental points using the transfer matrix method, and some opto-electronic properties of a monolayer of MoS_2 are probed in a phototransistor.

Resumen

Alejandro ANDRÉS JUANES

TMD-based optoelectronic devices

El estudio de materiales bidimensionales está en boga en los últimos tiempos dadas las características de éstos, que los hacen útiles para futuras aplicaciones muy prometedoras en el campo de la nanoelectrónica, la fotónica y la optoelectrónica. En concreto, está siendo extensamente estudiada la familia de los dicalcogenuros de metales de transición (TMDs – de sus siglas en inglés). El delgado espesor de las monocapas hace que el estudio de dispositivos fabricados con ellas sea de un interés fundamental.

Entre los desafíos principales de la investigación con materiales 2D se encuentran obtener e identificar monocapas. En este trabajo se describe un método para agilizar la identificación óptica de monocapas y estructuras de pocas capas mediante un microscopio óptico y se compara con la identificación *via* espectroscopía Raman. En primer lugar, se introducen los conceptos de materiales 2D, TMDs y las técnicas utilizadas para fabricar un dispositivo: exfoliación mecánica y transferencia de flakes con un polímero viscoelástico. Después, se explica el proceso de identificación óptica, cómo se toman las fotografías y cómo se miden los contrastes; así como la técnica de espectroscopía Raman y cómo distinguir cristales con distinto número de capas a partir de los espectros. Por último, los datos son comparados con un sencillo modelo numérico para la transmitancia de luz a través del material hecho aplicando el fundamento de la matriz de transferencia; y se muestran medidas eléctricas realizadas en un fototransistor con una monocapa de MoS_2 como canal.

Contents

Abstract II

1. Introduction 1
1.1. Transition metal dichalcogenides 2
1.2. Mechanical exfoliation. Viscoelastic stamping 5

2. Optical characterization technique 7
2.1. Workspace and setup 7
2.1.1. Microscope settings and characteristics 7
2.1.2. LEDs illumination panel 8
2.2. Image processing and measurement 8

3. Raman spectroscopy 12
3.1. Micro Raman Spectrometer 12
3.2. Raman spectra 14

4. Transfer Matrix Method (TMM) 16
4.1. Transfer Matrix for a consecution of media 17
4.2. Comparison with experimental data 18

5. Electrical measurements in a single layer MoS_2 phototransistor 20
5.1. Field-Effect Transistor 20
5.1.1. Phototransistor. Photocurrent and photogating 21
5.2. Photocurrent dependance on the incoming light power 22

6. Conclusions 24

A. Python scripts 26
A.1. Acquisition of transmittance from an image 26
A.2. Transfer Matrix Method calculation 28

Bibliography 31

List of Figures

1.1. (a) 2D materials piled up to form a van der Waals heterostructure, (b,c) analogy with pieces of LEGO®. Extracted from (Geim and Grigorieva, 2013). 2
1.2. MoS_2 monolayer molecular structure from different views. (a) 3D view, (b) top view showing a honeycomb-like lattice geometry and (c,d) profile views. Extracted from (*Molybdenum Disulfide (MoS2):Theory Applications* 2021). 3
1.3. Schematic view of the valence and conduction bands in an indirect- (a) or direct-bandgap (b) semiconductor. $h\nu$ symbolizes the energy of the absorbed photon and $h\Omega$ the one of a phonon. In the indirect-bandgap case, a 3 body interaction is needed. 4
1.4. Viscoelastic stamping process. (a) Crystal of MoS_2 being peeled off with blue tape, (b) schematic view of the small flakes (not scaled) attached to the tape, (c) transfer to the PDMS sheet and (d) optical microscope image (20x) of the flakes on top of the PDMS. 5
1.5. Illustration of a 300 nm SiO_2 substrate (a). In (b) the same substrate over a stage, and the PDMS attached to the glass slide to proceed to the all-dry deterministic transfer. 6

2.1. Different contrast observed when using the transmission mode (a) or the reflection mode (b). In both cases it was used the 100x objective. The monolayer is pointed with 1L. 8
2.2. Leica DM8000 Optical Microscope inside Nanotech USAL Cleanroom. 9
2.3. Screenshot of the program to measure the transmittance. The black squares are the areas selected to measure the intensity of the background (left) and flake (right) in the spot a of Fig. 2.4. 10
2.4. Image of the flake measured without the filter (a), and with the green filter (b) using the 100x objective. In the latter, points a-e where we the transmittance has been measured are marked. . 11

3.1. LabRAM HR Evolution Raman spectrometer, located in the I+D+i premises. The main parts are labeled in the image. The laser beam travels inside the spectrometer through a complex system of filters and mirrors. 13

3.2. (a) From bottom to top: spectrum in spot (a), (b), (c), (d) and (e) of Fig. 2.4. E^1_{2g} and A_{1g} are the main Raman modes. Spectra have been stacked for clarity. (b) Variation of the distance between the peaks with the number of layers. Extracted from (Buscema et al., n.d.). 14
3.3. Transmittance plotted against thickness of the flake. The thickness is calculated as the number of layers · 7 nm and the errorbars are the resulting standard deviation of 5 measures taken at each point. 15

4.1. Schematic view of the different coefficients. 16
4.2. Comparison between the experimental points (blue) and the numerical calculation (green). The shaded area includes all the possible values of $n + i\kappa$ within a range of $\pm$ 10% of their nominal value. 19

5.1. (a) Schematic view of a transistor. Source and Drain are Ti-Au contacts, and the base of Si is the Gate electrode. (b) IV characteristic of the transistor. (c) Comparison between light on (orange) and off (blue) current flow with $V_{ds} = 2.5V$. 21
5.2. (a) Current over time applying different laser powers.(b) the points fit to a curve $I_{PC} = kP^{\alpha}$ with $\alpha = 0.53$. 23

List of Tables

2.1. Transmittance in each point with respect to the background. The transmittance corresponds to the mean of five independent measurements. The Δ column is the standard deviation of the set of measurements. 11

3.1. Position of the Raman peaks E and A. Δf is the distance between them. All values are expressed in cm^{-1}. 15

Key words

TMDs, 2D materials, Raman spectroscopy, MoS_2, Transfer Matrix

Palabras clave

TMDs, materiales 2D, Espectroscopía Raman, MoS_2, Matriz de transferencia

Objectives

The aim of this project is the development of a method to identify monolayers of 2D materials in a more agile way in order to build nanodevices based on them.

Objetivos

El objetivo de este trabajo es desarrollar un método de identificación óptica de monocapas de materiales 2D que permita agilizar el proceso de fabricación de dispositivos.

«*¿Pero es posible trabajar en algo serio y duradero, olvidando el enorme misterio del universo y sin inquirirlo?*»

Miguel de Unamuno.

1 Introduction

During the last century, modern societies have been immersed in the so-called third industrial revolution represented by electronics and microelectronics. The latter is based on semiconducting materials (mainly silicon) whose behavior we can understand thanks to the development of Quantum Mechanics (Aitken, 1979). In 1960, Richard P. Feynman during his lecture *There's plenty of room at the bottom*(Feynman, 2011) prophesized about the huge possibilities the new paradigm of quantum laws would open up. He asked himself "What could we do with layered structures with just the right layers?". Because few-dimensional structures (i.e. 1D-nanowires and 2D-layers) where nothing but a theoretical tool used for learning (Landau, 1937). However, that changed when Novoselov, Geim and others demonstrated that it was possible to manipulate a single atomic layer of the nowadays well-known *graphene* and measure electronic transport on it (Novoselov et al., 2004). The reason why this works is because bounds between atoms in this 2D materials are asymmetrical, being strong covalent bounds between atoms in the same layer and weak electrostatic (van der Waals - vdW) bounds between layers. Especifically, monolayers of different vdW crystals can be piled up building vdW heterostructures (Fig. 1.1).

2D layered materials have unique and tunable material properties that can be engineered to solve fundamental scientific and technological challenges. Their chemical, optical and electrical properties can be modified, for example, by their interaction with the media thanks to their inherent large surface-to-volume ratio. One of those challenges is to overpass the CMOS scaling limit. Moore's law predicts how the number of transistors in a microprocessor grows as the fabrication technologies improves, but there is a physical limit, though. To avoid short-length channel issues, it is needed that the channel length L_{CH} fulfills the mathematical relationship $L_{CH} < 3\lambda$ where $\lambda \propto t_{CH}^{\frac{1}{2}}$ and t_{CH} is the thickness of the material serving as the channel of the transistor. Immediately emerges the benefit of integrating 2D materials in Silicon chips due to their thin nature. Nevertheless, a lot of research in contact engineering needs to be done because the performance of this transistors will ultimately be limited by contact resistance (Das et al., 2015).

Another areas of action for these atomically thin materials are Optics and Optoelectronics. They will appear new switches, memories, signal-amplifiers, light-related sensors,etc. Their characteristics make them extremely desirable for next-generation display technologies. They are mechanically flexible, due

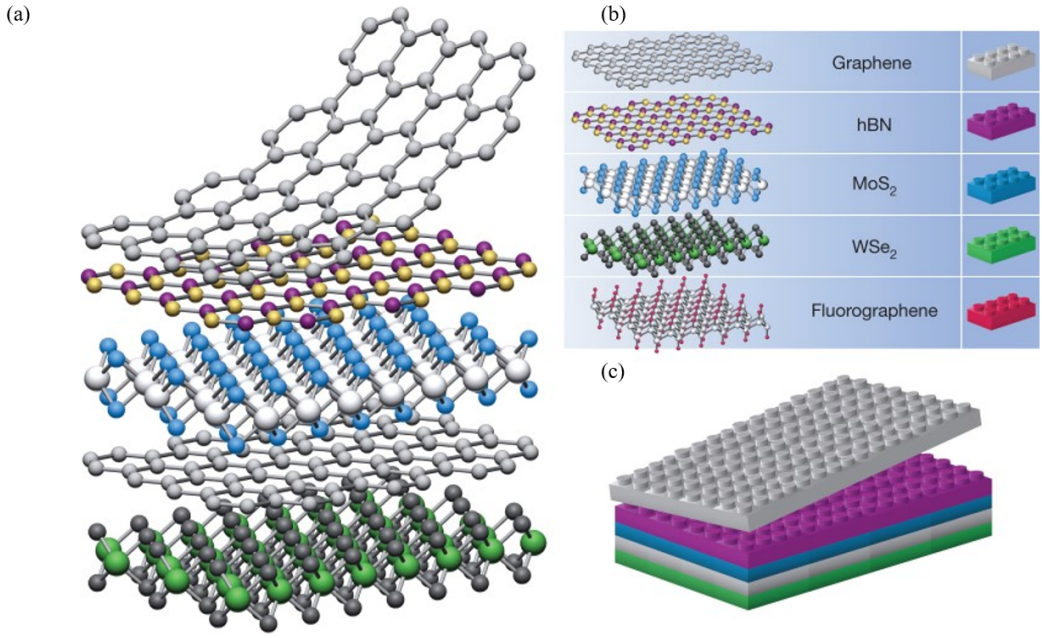

FIGURE 1.1: (a) 2D materials piled up to form a van der Waals heterostructure, (b,c) analogy with pieces of LEGO®. Extracted from (Geim and Grigorieva, 2013).

to their vdW epitaxy and are optically transparent because most of the incident light is transmitted through. Indeed, the former has open a new line of research in straintronics (Wei, Dai, and Huang, 2017; Bukharaev et al., 2018).

Due to the importance of the study of single and few-layers of these materials, in this work I will describe a method for a simple and fast optical characterization of them. This will be done combining the study of the transmittance of light throughout them (see Chapter 2) and their Raman scattering response (see Chapter 3). In Chapter 4, a theoretical model for the transmittance will be proposed and the numerical results will be compared to the experimental data. Finally, the electrical response of a device will be displayed in Chapter 5.

1.1. Transition metal dichalcogenides

Among others, a family of promising 2D materials are transition metal dichalcogenides (TMDs) which follow the formula MX_2 where M is a transition metal atom (e.g. Mo,W,Ta,...) embedded in the middle of two chalcogen layers X (e.g. S,Se,Te,...). Whereas graphene is a zero-band-gap semiconductor, meaning the distance between its valence and conduction band (VB and CB, respectively) in the energy space is null, bulk semiconducting TMDs usually behave as an indirect-band-gap semiconductors (i.e. maximum of the VB is not aligned with the minimum of the CB at the same momentum $\mathbf{k}$. Nonetheless, when reducing the number of layers a indirect-to-direct-band-gap transition occurs (Das et al., 2015). In consequence, electronic band transitions

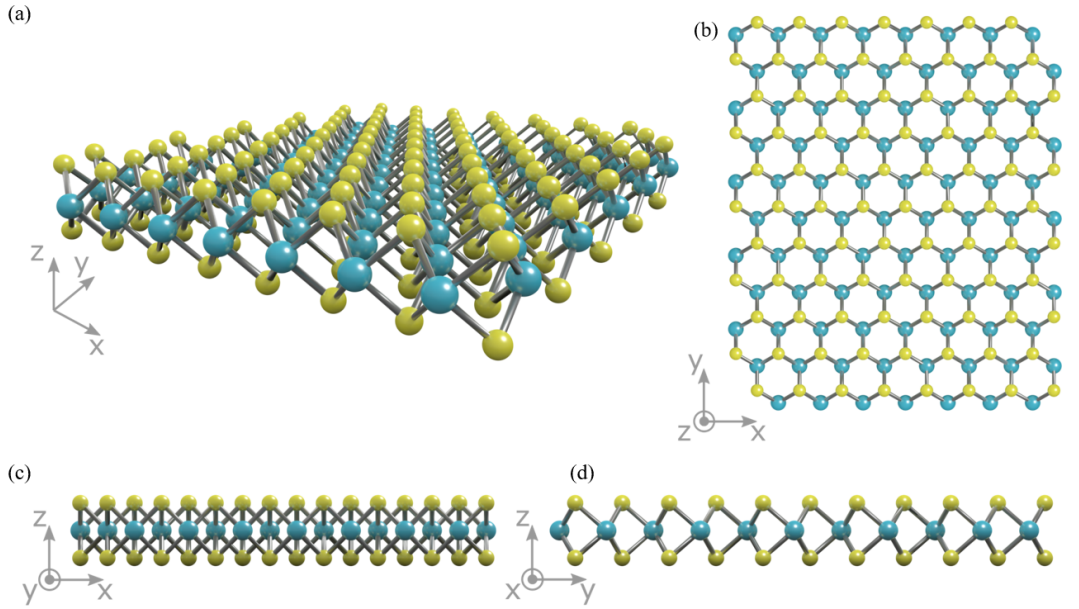

FIGURE 1.2: MoS_2 monolayer molecular structure from different views. (a) 3D view, (b) top view showing a honeycomb-like lattice geometry and (c,d) profile views. Extracted from (*Molybdenum Disulfide (MoS2):Theory Applications* 2021).

are more likely to occur in direct-band-gap semiconductors because it is only necessary for the electron in the VB to gain a determined amount of energy greater than the band-gap energy E_g. For an indirect-band-gap transition a change in the momentum of the electron is also needed, making this transitions less probable.

For technological applications, TMDs will be useful because their band-gap energies are related to visible wavelengths (Choi et al., 2017). For a band-gap energy of $E_g \sim 2eV$,

$$\lambda = \frac{hc}{E_g} = \frac{2\pi\hbar c}{E} \sim \frac{6}{2eV} \cdot 197eV \cdot nm \sim 600nm.$$

Photoluminescence is the emission of light from any object after the absorption of radiation. Microscopically, each photon corresponds to the transition of an electron from the CB to the VB. In the case of 1L MoS_2, the direct gap is associated with an intense photoluminescence signal that can be of great interest for technological applications. The rise of 2D TMDs has significantly advanced the study of spin, valley pseudospin and many other degrees of freedom such as layer pseudospin. Following theoretical discoveries of the intrinsic physical properties associated with valley pseudospin, rapid experimental progress has been made in the control of valley polarization and coherence that allows manipulation in ways similar to real spin (Xu et al., 2014). Specifically, monolayer TMDs with a direct bandgap offer unprecedented opportunities to explore semiconductor optics in the 2D

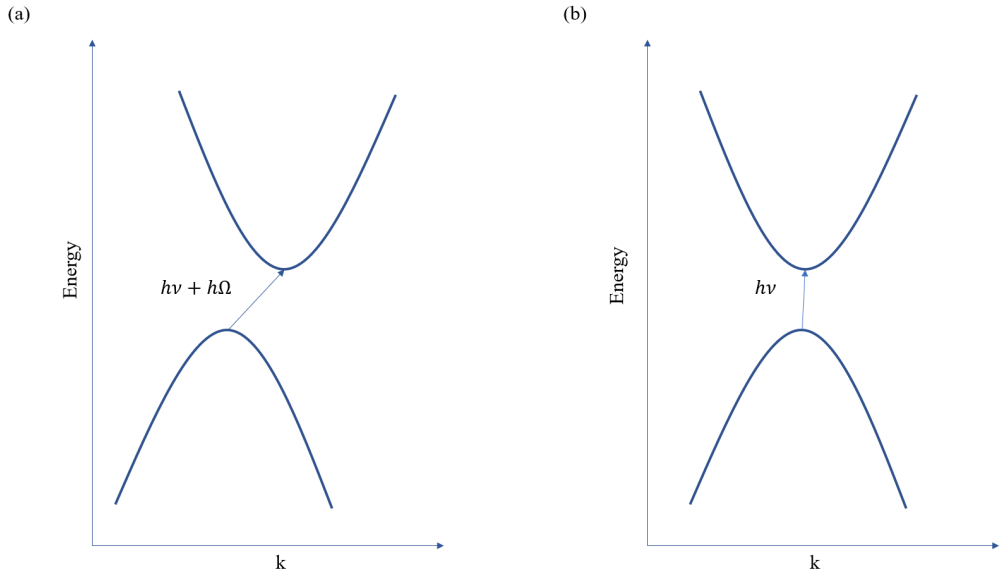

FIGURE 1.3: Schematic view of the valence and conduction bands in an indirect- (a) or direct-bandgap (b) semiconductor. $h\nu$ symbolizes the energy of the absorbed photon and $h\Omega$ the one of a phonon. In the indirect-bandgap case, a 3 body interaction is needed.

limit. The signature of strong spin-orbit coupling (SOC) has been observed in optical absorption spectra, with two main excitonic features, A and B excitons associated with the two spin-split VB in the $\pm$K valleys (Vaquero et al., 2020). Moreover, the most distinctive property of 2D TMDs is perhaps the strong coupling between spin and the different pseudospins of carriers. It is expected that the interplay between these quantum DoFs in various geometries, including heterostructures and quantum wires, will reveal many novel physical phenomena (Das et al., 2015).

In this work, MoS_2 will be the material of study. It is one of the most studied 2D semiconductors. Single-layer MoS_2 has a unique quantum luminescence efficiency and exhibits a high channel mobility ($\sim 200 cm^2 V^{-1} s^{-1}$) and current ON/OFF ratio (1×10^8) used as a channel in a field-effect transistor (FET). Efficient single layer MoS_2 phototransistors have also been studied (Yin et al., 2012) obtaining better responsivity results than in a graphene-based device. Photodetectors based on this material are not only plausible but they can offer additional advantages in contrast to the existing possibilities because of its transparency, mechanical flexibility and easy processing (Koppens et al., 2014).

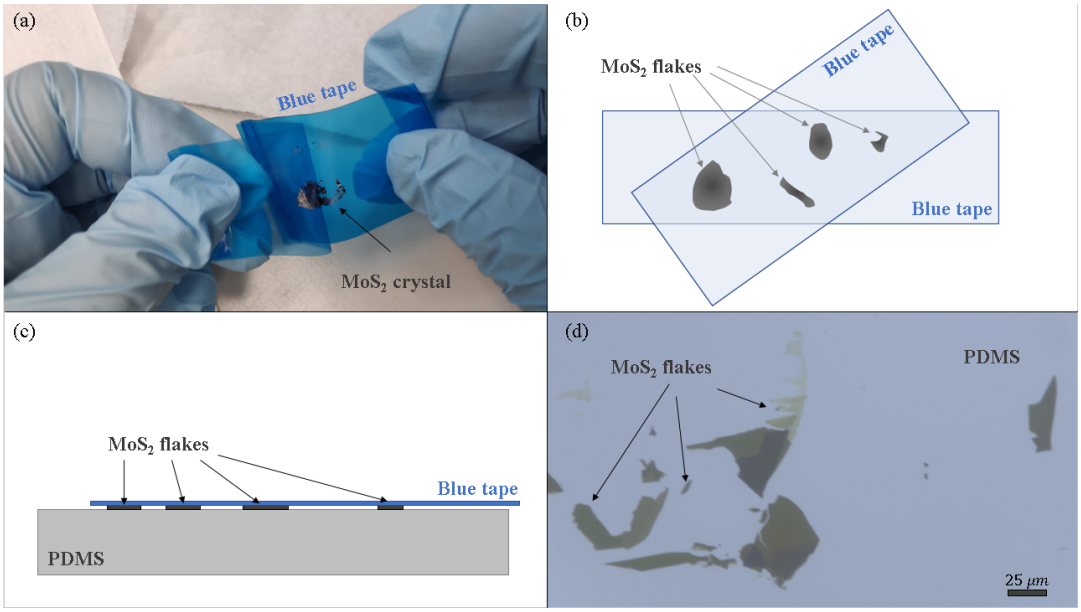

FIGURE 1.4: Viscoelastic stamping process. (a) Crystal of MoS_2 being peeled off with blue tape, (b) schematic view of the small flakes (not scaled) attached to the tape, (c) transfer to the PDMS sheet and (d) optical microscope image (20x) of the flakes on top of the PDMS.

1.2. Mechanical exfoliation. Viscoelastic stamping

There are various methods of obtaining monolayers. The first MoS_2 (circa 1986) (Joensen, Frindt, and Morrison, 1986) was achieved via chemical exfoliation using Li intercalation to separate the sheets in a solution. However, the most common method used to manufacture devices for research is mechanical exfoliation. To exfoliate flakes, which are small crystals, from bulk crystals synthesized via chemical vapour transport and create the device measured in Chapter 5, I used the all-dry viscoelastic stamping method (Castellanos-Gomez et al., 2014). It consists in peeling off part of the crystal by an adhesive tape. After that, the peeled sheet is detached on a piece of polydimethylsiloxane (PDMS), which is a viscoelastic material. Thanks to its viscoelastic properties, and with a little pressure smoothly applied with a finger the PDMS can penetrate the interface between the flakes and the adhesive tape. Then if the tape is retired rapidly, the PDMS cannot recover its original shape and drags the flakes with it (Fig. 1.4). In this stage of the process, we would be ready to analyze the flakes with the optical microscope (see Chapter 2). This exfoliation method produces flakes with different sizes and thicknesses randomly distributed over the PDMS. Among all flakes, one shall select the one whose geometry and thickness fit well with the purpose of the device.

Now, it can be transferred to a substrate using the deterministic transfer method (Castellanos-Gomez et al., 2014). In this case, we used a 300nm width silicon-SiO_2 wafer. The sample is attached to a glass slide and turned upside

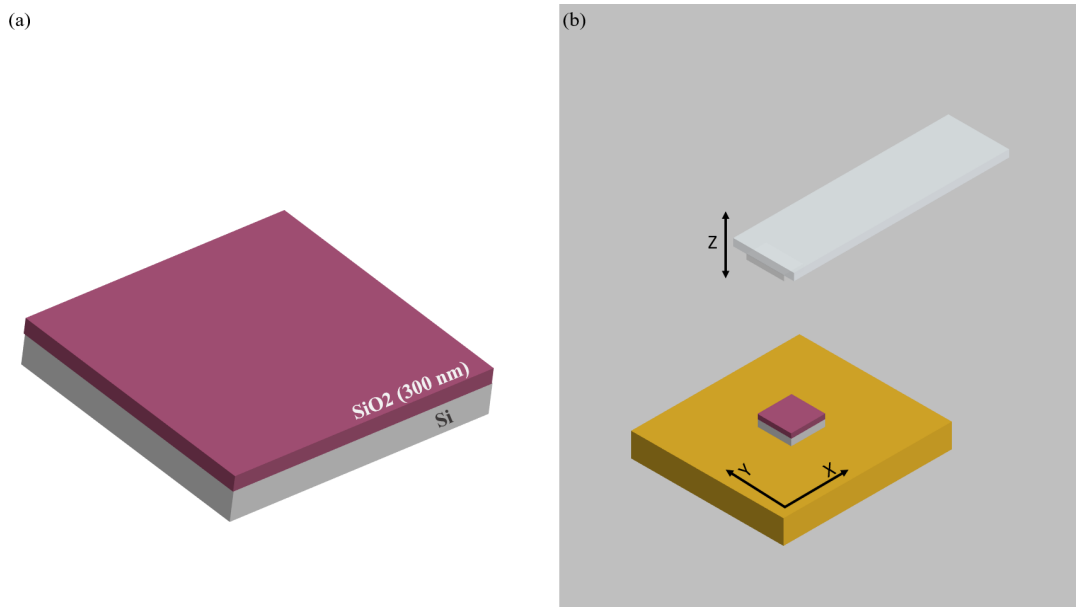

FIGURE 1.5: Illustration of a 300 nm SiO_2 substrate (a). In (b) the same substrate over a stage, and the PDMS attached to the glass slide to proceed to the all-dry deterministic transfer.

down, facing the SiO_2 substrate. The substrate is placed in a stage that can be moved in the XY plane in displacements of microns, which allow us to control the relative position of the flake and the region of the substrate where we want to stack it[1]. In our case, the sample is sandwiched in between two flakes of hBN, a TMD that behaves as an insulator.

The final step consist on creating the contacts that will permit us to measure the electrical properties of the material. To do so, gold and titanium are evaporated onto the sample. But, prior to that we create a mask using a resin and electron beam lithography. This allows us to give the contacts a geometry of our election. This process is carefully explained in (Clericò et al., 2020).

[1]This is very important when creating heterostructures (Geim and Grigorieva, 2013), where flakes of different materials are piled up. It is necessary also to create twisted bilayer graphene (Mogera and Kulkarni, 2020).

2 Optical characterization technique

Flakes of MoS_2 are exfoliated and transferred to PDMS layers using the technique described before (section 1.2). If the transfer is completed successfully, the flakes can be examined through transmission optical microscopy and determine in such way directly their shape. Nevertheless, as it has been commented previously, their thickness cannot be determined *a priori* only by exploration with the microscope. Thin films can be selected *grosso modo* due to their low contrast and then we can determine the exact number of layers with a high level of precision up to 4-5 layers using Raman spectroscopy (see Chapter 3). The aim of this project is to correlate the optical transmittance (defined as the portion of light passing through the flake of the incident light) with the thickness of the flake to directly find few-layered flakes with the microscope which would permit the users of these premises to faster prepare their devices.

2.1. Workspace and setup

The optical microscope can be used principally in two ways. One can illuminate the sample from above and see the light reflected by the sample (as when one use a spyglass or a pair of binoculars) or light can come from under the sample and what camera's objective or our eyes will capture the shadow of the sample (imagine a show of shadow puppets). Experience show that the latter gives more contrast when looking for thin flakes (see Fig. 2.1). An optical microscope mounting a 100x objective is used to take the pictures. It does not have an inherent transmission mode. Fortunately, the samples can be placed over a LEDs panel and switching off the light-bulb of the microscope a transmission mode can be made up (Fig. 2.2). After that, the images taken are processed using a python script. The python code can be found in the Appendix.

2.1.1. Microscope settings and characteristics

A Leica DM8000 Optical Microscope was used to take the pictures of the flakes. Though pictures were taken with a 100x objective, the microscope has a 5x, 10x, 20x and 50x magnification. These objectives are very useful to find the region of study within the whole PDMS sheet because they reach a wider field. Usually, pictures with the different zooms are taken in order

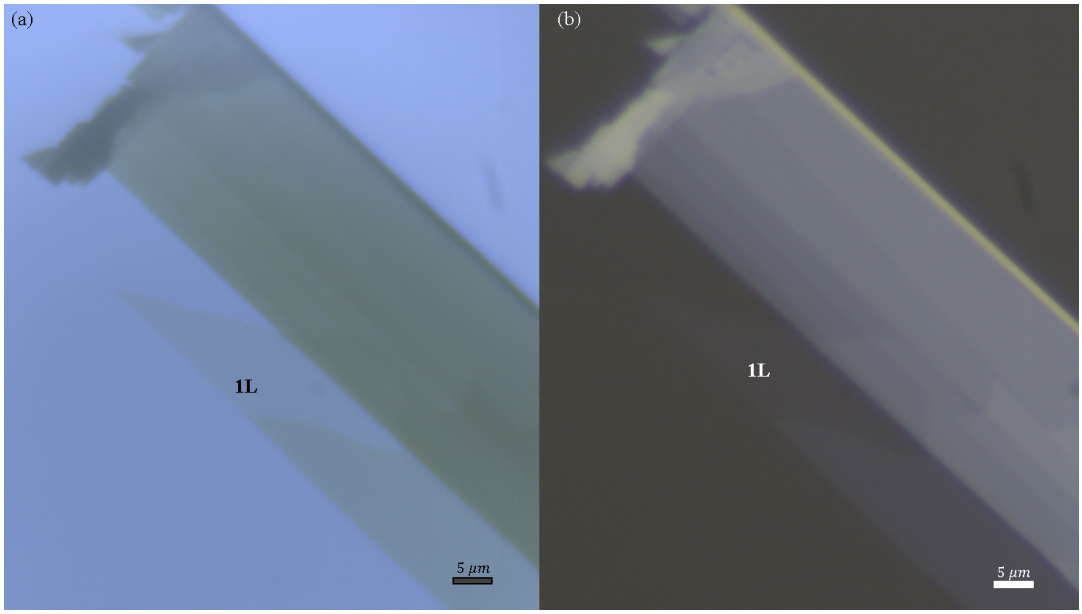

FIGURE 2.1: Different contrast observed when using the transmission mode (a) or the reflection mode (b). In both cases it was used the 100x objective. The monolayer is pointed with 1L.

to easily find the desired flake later. It has LED illumination integrated that can be used in Reflection mode, a stage that can be moved in the X,Y and Z directions (the vertical distance to the lens is changed to focus the sample), a green light filter, a CCD sensor to take the pictures, a motorized aperture diaphragm and many other automated elements that can all be controlled with its native software.

2.1.2. LEDs illumination panel

The performance of the LEDs panel is finite. Though it is a very witty and inexpensive idea, the power is a little bit low when using an objective with low numerical aperture. Moreover, while the pre-processing of the images it showed up that the light is not uniform and the deviation is greater than the contrast of the monolayers. This could play an important role if we wished to automate the process but as the measurements will be taken manually, this problem can be sidestepped. The measurement process is detailed below. (imagen background?)

2.2. Image processing and measurement

An image in the screen of our computer is the result of thousands of thousands of little spots called *pixels* (acronym of picture element). Each color is then obtained by the sum of normally 3 colour intensities (i.e. **R**ed, **G**reen and **B**lue in the **RGB** system). For the computer, the information of these intensities is stored in a $(a \times b \times 3)$ matrix where $a \times b$ are the number of lines and columns of pixels in which the image is subdivided and 3 recalls to the

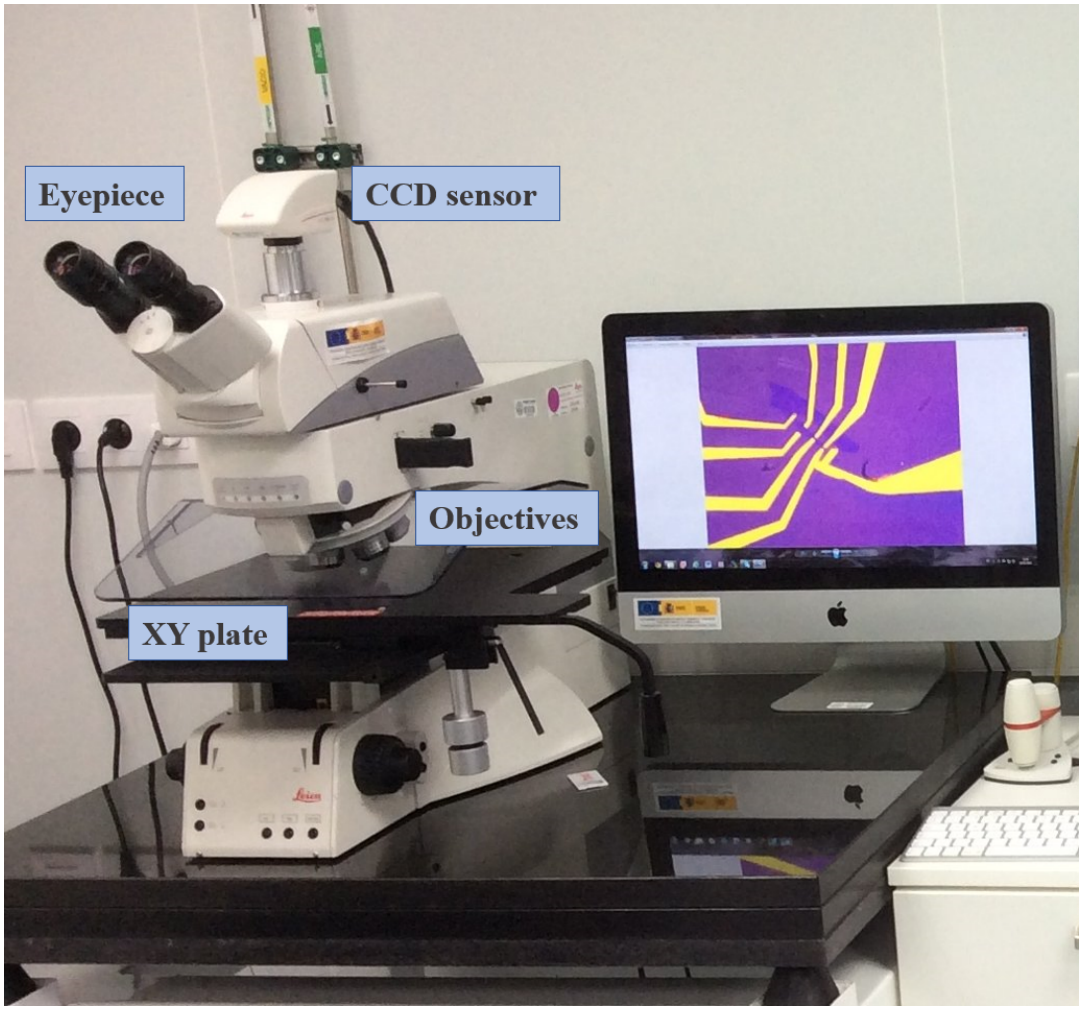

FIGURE 2.2: Leica DM8000 Optical Microscope inside Nanotech USAL Cleanroom.

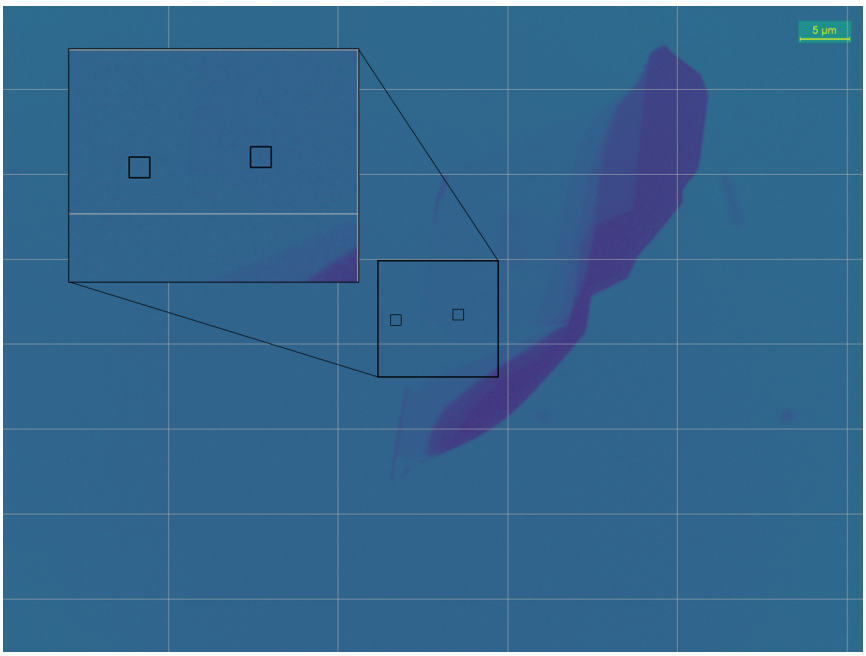

FIGURE 2.3: Screenshot of the program to measure the transmittance. The black squares are the areas selected to measure the intensity of the background (left) and flake (right) in the spot a of Fig. 2.4.

3 different channels. The first step in pre-processing the image is select only one of this channels to work with it (Taghavi et al., 2019). I chose the green because the contrast was greater than with the others, but as long as the election is consistent, it is indifferent which to work with. Therefore, we have a (1920x2560) matrix.

Now, we select two points, one in the background and the other in the desired flake and compute the ratio of the pixels intensities at these two points. Due to the low intensity of the incoming light through the objective, the images have a low signal-to-noise ratio. For that reason, the intensity of the pixels that is used to compute the transmittance ratio is the mean of a square of 30x30 pixels (see Fig. 2.3). To avoid problems with the changing intensity of the background, it is preferable to choose a region near the edge of the flake. In addition, to reduce systematic measurement error each flake is measured 5 different times selecting different couples of points. The uncertainty in the measurement of the transmittance can be approximated calculating the standard deviation correspondent to the set of measures in each point. The results are in Table 2.1.

It must be noted that we consider pictures taken using the whole visible light spectrum, which give good results from a qualitative and practical point of view. To compare with the theoretical calculation of chapter 3 I took monochromatic pictures. If one would like to compute the theoretical transmittance (as it is done in chapter 4), it will be needed to consider not only the frequency dependence in the CCD camera sensor, as well as the shape of the spectrum of the LEDs panel; but also the dependence in the refractive index

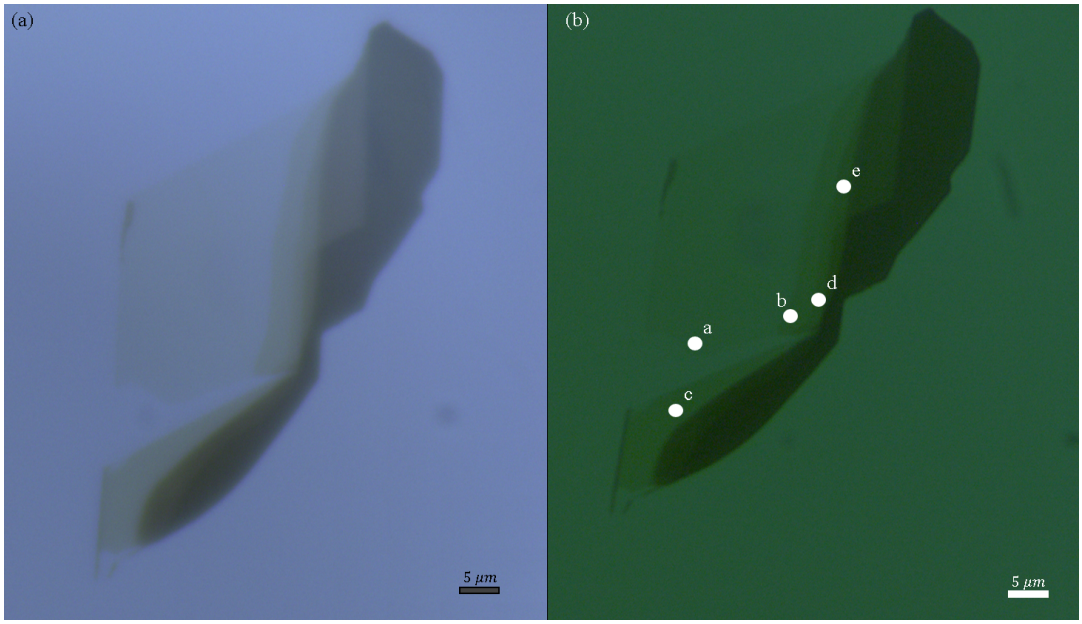

FIGURE 2.4: Image of the flake measured without the filter (a), and with the green filter (b) using the 100x objective. In the latter, points a-e where we the transmittance has been measured are marked.

of the material (i.e. $\tilde{n}(\omega) = n(\omega) + i\kappa(\omega)$). This, though it is not impossible, is tedious and out of the scope of this work. To simplify this calculation, pictures in the microscope were taken with a narrow band filter that only let green light (530 nm) pass throughout it. See that in agreement with all the previous considerations, the transmittance values may change.

In fact, it has been demonstrated numerically and experimentally that the transmittance depends on the wavelength using a SiO_2 substrate. In some cases, due to interference processes, the transmittance may be greater than that of the background.

Spot	Transmittance	Δ
a	0.974	0.018
b	0.924	0.013
c	0.914	0.002
d	0.850	0.03
e	0.820	0.011

TABLE 2.1: Transmittance in each point with respect to the background. The transmittance corresponds to the mean of five independent measurements. The Δ column is the standard deviation of the set of measurements.

3 Raman spectroscopy

Raman Spectroscopy is a non-destructive analysis technique which provides detailed information about chemical structure, phase and crystallinity and molecular interactions. It is based upon the interaction of light with the vibrational modes of a material. It is a light scatter technique, whereby a molecule scatters incident light from a laser. Most of the scattered light has the same wavelength of the incident one and does not provide information (Rayleigh Scattering). However, a small amount of photons (around 1 in 1.000.000.000 – this is equivalent to 7 people among the whole Earth population) is scattered at slightly different wavelengths. It is widely used in biology, because it allows the researchers to do *in-vivo* measurements of cells and tissues, and it is also commonly used among the 2D community because the Raman spectra of the different 1 layer (1L), 2L, 3L ... structures can be used to characterize each of them (*What is Raman Spectroscopy? - HORIBA* n.d.).

In the case of MoS_2, the Raman spectrum shows two main Raman-active modes, ${E_{2g}}^1$ and A_{1g}. Whereas the former represents an in-plane vibration, the latter corresponds to an out-of-plane lattice expansion (Zhou et al., 2014). In this chapter, it will be used the distance between the two peaks of these modes is a good parameter to characterize the number of layers.

3.1. Micro Raman Spectrometer

Spectra were acquired with a LabRAM HR Evolution Raman spectrometer. It offers the possibility to do micro and macro measurements. A Ventus Solo laser emitting at 532 nm and with an output power of 100mW was used. Due to the small scale of the flakes, the 100x objective was mounted to produce a laser spot of around 1 μm^2 when focused. Moreover, if the laser were focused on the sample in this bare configuration, it would burn out the flakes due to the high power reached in the laser spot. To avoid any damage, the laser beam goes through a filter that reduces the intensity to 0.01, 0.1, 0.5% ... of its initial intensity. It has a motorized stage in the XY plane with a 0.05 μm step that enables to perform fast confocal measurements, as well as maps of spectra over an entire region. The backscattered light is collected by the same objective that focuses the exciting beam and then separated by a diffraction grating and collected with a Synapse CCD detector. Two different gratings can be chosen, 600 and 1800 grooves/mm, which reflects on the bandwith and definition needed. As the signal is quite low, the detector is cooled with a Peltier effect device, which reduces the thermal noise of the different pixels.

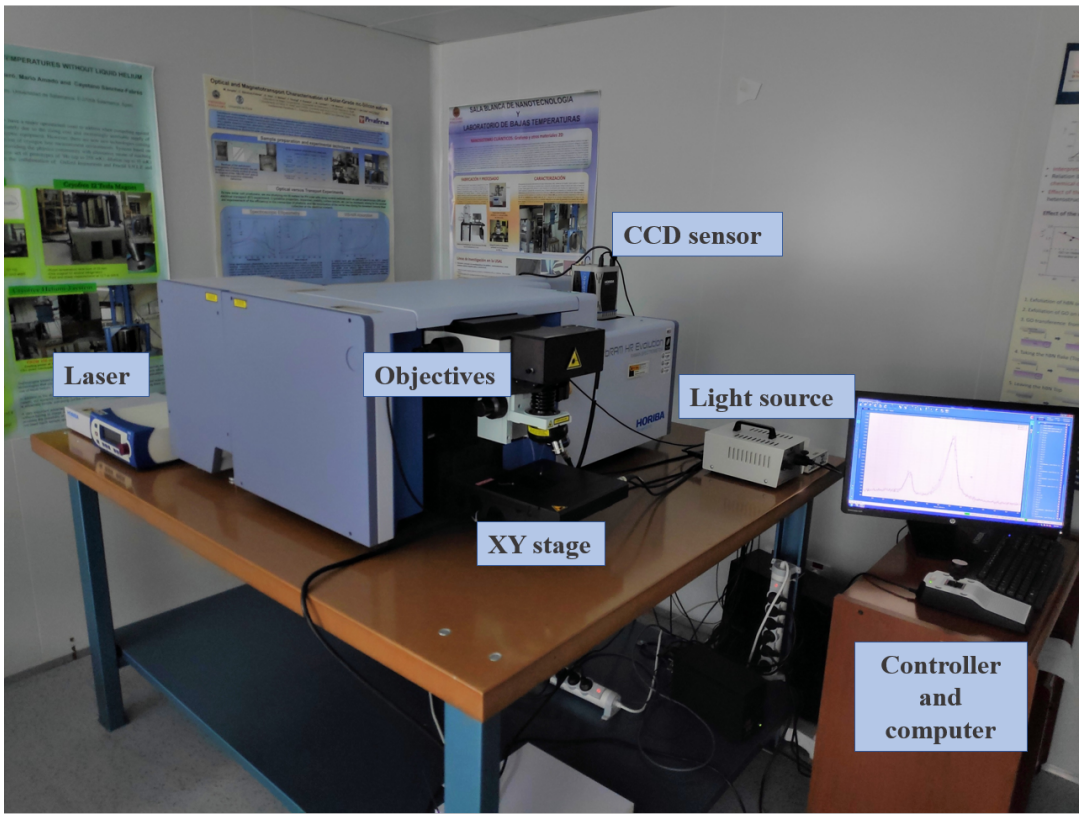

FIGURE 3.1: LabRAM HR Evolution Raman spectrometer, located in the I+D+i premises. The main parts are labeled in the image. The laser beam travels inside the spectrometer through a complex system of filters and mirrors.

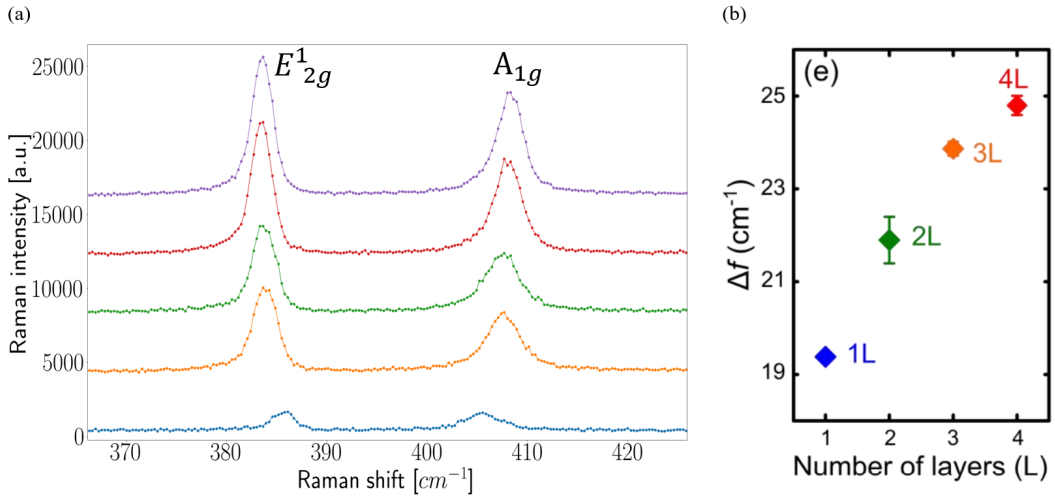

FIGURE 3.2: (a) From bottom to top: spectrum in spot (a), (b), (c), (d) and (e) of Fig. 2.4. E^1_{2g} and A_{1g} are the main Raman modes. Spectra have been stacked for clarity. (b) Variation of the distance between the peaks with the number of layers. Extracted from (Buscema et al., n.d.).

3.2. Raman spectra

The following setup was selected to acquire each spectrum:

- Diffraction grating: 1800 grooves/mm
- 0.5% intensity filter
- Centered at 400 cm^{-1} of Raman shift
- Number of measurements: 10
- Exposition time (1 measurement): 4 seconds

In the flake of the Fig. 2.4 we focused the laser at those 5 spots (a),(b),(c),(d),(e). The results of the measurements are shown in Fig. 3.2. The y-axis corresponds to the counts of photons scattered at the different wavelengths, while the x-axis is the Raman shift, i.e. the difference of frequency between the original laser photons and the backscattered photon. It can be seen that as the number of layers is incremented, the peaks around 400 cm^{-1} separate. In each spectrum, the peak at $\sim$ 385 cm^{-1} corresponds to the $E_{2g}{}^1$ mode and the one at $\sim$ 405 cm^{-1} to the A_{1g} mode. In addition, it is seen that in all cases there is a peak in 483 cm^{-1} that does not change in position, and its magnitude reduces as the number of layers increase. It is presumably related to the substrate of PDMS.

The position of the flakes is heavily influenced by the environment, the substrate, the temperature and many more factors. Yet, as it was commented previously, the distance between both peaks is a good parameter to characterize the number of layers of the flake (up to 4-5 layers). Each peak can be

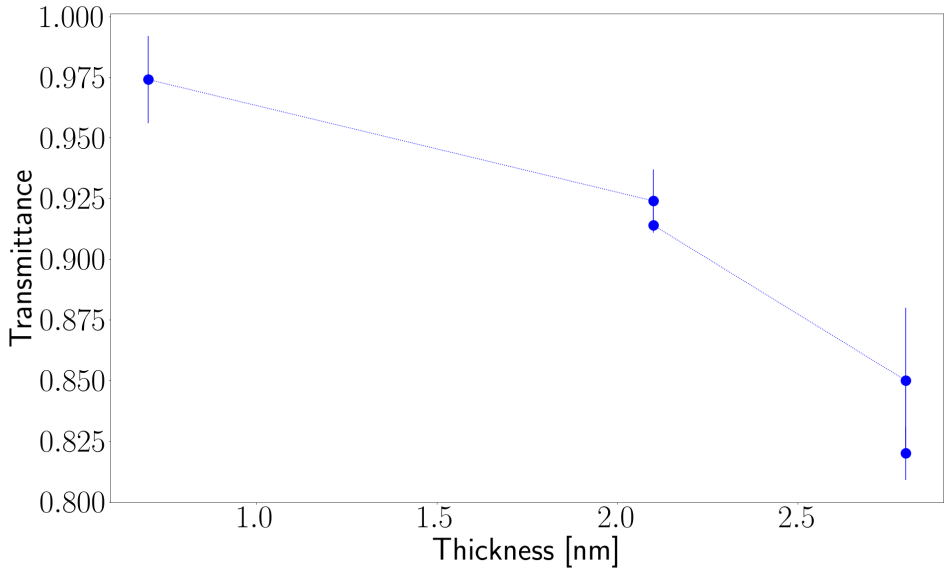

FIGURE 3.3: Transmittance plotted against thickness of the flake. The thickness is calculated as the number of layers · 7 nm and the errorbars are the resulting standard deviation of 5 measures taken at each point.

fitted to a Lorentzian curve and from the fitting can be extracted the position of the peaks. Nevertheless, if the position of the higher value is accounted, the results obtained are sufficiently good for the purpose of this work. The results are displayed in Table 3.1.

Spot	E mode	A mode	Δf	Number of layers
a	386.0	405.6	19.6	1
b	384.0	407.5	23.5	3
c	383.6	407.7	24.1	3
d	383.6	408.0	24.4	4
e	383.6	408.3	24.7	4

TABLE 3.1: Position of the Raman peaks E and A. Δf is the distance between them. All values are expressed in cm^{-1}.

Comparing with the literature, each point (a)-(e) can be characterized (Buscema et al., n.d.). It is noted that the regions with different layers in Fig 2.4 are of the same size of the laser spot, which makes that some of the photons measured would not correspond to the desired region. Now, gathering the results of the transmittance obtained in Chapter 2 and knowing already the number of layers, it can be plotted the relationship between transmittance and flake thickness. It is only left to know that the thickness of a layer is $\sim$ 7 nm (Li and Zhu, 2015), which has been measured using an Atomic Force Microscope (AFM). The result is shown in Fig 3.3.

4 Transfer Matrix Method (TMM)

In this chapter, a theoretical model is described and computed using the Transfer Matrix formalism. Later on, its results will be compared to those obtained of the observations.

TMM allows us to connect amplitudes at one side of a scattering region with the amplitudes at the other. In our problem, such amplitudes will be those of the incoming, reflected and transmitted light. Let them be the complex amplitudes a whose direction is ingoing the scattering region and b outgoing; and use the subindex i (j) meaning before (after) having passed through the scattering region (recall that our problem is one-dimensional in the physical space). On the one hand, the relation at the interface between two media i and j with different complex refractive index $\tilde{n} = n + i\kappa$ can be written in matrix notation as

$$\begin{pmatrix} a_j \\ b_j \end{pmatrix} = S_{ij} \begin{pmatrix} a_i \\ b_i \end{pmatrix} \tag{4.1}$$

where S_ij is the Scattering matrix. The elements of the matrix S_{ij} are related to the Fresnel's coefficients in the case of normal incidence,

$$t_{ij} = \frac{2\tilde{n}_i}{\tilde{n}_i + \tilde{n}_j} \tag{4.2}$$

and

$$r_{ij} = \frac{\tilde{n}_i - \tilde{n}_j}{\tilde{n}_i + \tilde{n}_j} = -r_{ji} \tag{4.3}$$

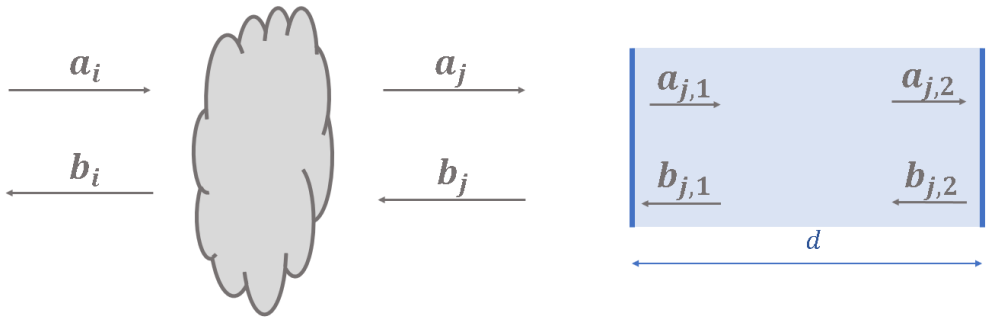

FIGURE 4.1: Schematic view of the different coefficients.

for the transmitted and the reflected beam, respectively. In terms of these coefficients, the relations between the amplitudes are

$$a_j = t_{ij}a_i + r_{ji}b_i$$

$$b_i = r_{ij}a_i + t_{ji}b_j.$$

By algebraic manipulations, one can easily isolate a_j and b_j in terms of a_i and b_i

$$b_j = \frac{1}{t_{ji}}(-r_{ij}a_i + b_i) = \frac{1}{t_{ji}}(r_{ji}a_i + b_i) \tag{4.4}$$

and substituting (4.4)

$$a_j = t_{ji}a_i + r_{ji}(\frac{1}{t_{ji}}(r_{ji}a_i + b_i)) = (t_{ij} + \frac{r_{ji}}{t_{ji}})a_i + \frac{r_{ji}}{t_{ji}}b_i. \tag{4.5}$$

Finally, developing the parenthesis

$$t_{ij} + \frac{r_{ij}^2}{t_{ji}} = \frac{2\tilde{n}_i}{\tilde{n}_i + \tilde{n}_j} + \frac{\tilde{n}_i + \tilde{n}_j}{2\tilde{n}_i} \cdot \frac{(\tilde{n}_i - \tilde{n}_j)^2}{(\tilde{n}_i + \tilde{n}_j)^2} = \frac{4\tilde{n}_i\tilde{n}_j + \tilde{n}_i^2 + \tilde{n}_j^2 - 2\tilde{n}_i\tilde{n}_j}{2(\tilde{n}_i + \tilde{n}_j)\tilde{n}_j} = \frac{\tilde{n}_i + \tilde{n}_j}{2\tilde{n}_j} = \frac{1}{t_{ji}}$$

we obtain

$$a_j = \frac{1}{t_{ji}}(a_i + r_{ji}b_i). \tag{4.6}$$

Hence,

$$S_{ij} = \frac{1}{t_{ji}} \begin{pmatrix} 1 & r_{ji} \\ r_{ji} & 1 \end{pmatrix}. \tag{4.7}$$

On the other hand, the light propagates throughout a medium j as a plane wave $e^{i\phi_j}$ where the phase corresponds to $\phi_j = \frac{2\pi}{\lambda}\tilde{n}_j d$, being d the thickness of the material. If we consider the positive and negative velocitiy waves,

$$\begin{pmatrix} a_{j,2} \\ b_{j,2} \end{pmatrix} = \begin{pmatrix} e^{i\phi_j} & 0 \\ 0 & e^{-i\phi_j} \end{pmatrix} \begin{pmatrix} a_{j,1} \\ b_{j,1} \end{pmatrix} = P_j \begin{pmatrix} a_{j,1} \\ b_{j,1} \end{pmatrix} \tag{4.8}$$

being P_j the Propagation matrix (Fig. 4.1).

4.1. Transfer Matrix for a consecution of media

Now, we are able to compute the Transfer matrix M that connects the amplitudes at one side and the other of a stack of materials. For a stack of N layers

$$\begin{pmatrix} a_{out} \\ b_{out} \end{pmatrix} = S_{N,N+1}P_N S_{N-1,N} \cdots P_2 S_{12} P_1 S_{01} \begin{pmatrix} a_{in} \\ b_{in} \end{pmatrix} \tag{4.9}$$

In order to compute the transmittance of the MoS_2 flakes, the following assumptions have been made:

- The thickness of the PDMS is sufficiently large so that we consider it the first medium. This will sidestep interference of the light inside the cavity of the PDMS, which does not occur because the thickness of the PDMS ($\sim 3mm$) is much greater than the coherence length of the LED display light.
- The many-layered flakes will be considered as a continuous *brick* of material with the monolayer's refractive index. The refractive index has been extracted from Zhang et al., 2015.
- Only light inciding normal to the interfaces contributes to the calculus, though the numerical aperture of the microscope objective might play a role collecting beams coming in other directions.

Finally, the transmittance will be the ratio between the transmitted power with PDMS and a flake, and only with PDMS. The coefficient of transmission t is equal to the m_{11}^{-1} being m_{11} the first element of the Transfer matrix. Note that in order to preserve conservation of energy in the interface, the power transmitted is

$$T = \frac{\tilde{n}_j}{\tilde{n}_i} \frac{1}{|m_{11}|^2}. \tag{4.10}$$

In this particular case, the Transfer matrix without flake corresponds simply to the Scattering matrix from PDMS to Air, whereas the Transfer matrix with a flake, particularizing (4.9) is

$$\begin{pmatrix} a_{out} \\ b_{out} \end{pmatrix} = S_{12} P_1 S_{01} \begin{pmatrix} a_{in} \\ b_{in} \end{pmatrix}$$

where the subindex correspond to the media: PDMS (0), MoS_2 (1) and Air (3).
Therefore, the Transmittance is

$$T = \frac{T_{flake}}{T_{PDMS}} \tag{4.11}$$

which can be computed for flakes of any thickness.

4.2. Comparison with experimental data

Using the setup of chapter 2, selecting only green light of $\lambda = 530nm$ and measuring the distance between the Raman peaks to characterize the different regions by their number of layers the following points where obtain, which can be compared to the model.

The model reproduces the descendent trend of the experimental points, even though it appears to be shifted to the left. Nevertheless, when a wider range of thickness is computed (Fig. 4.2), interesting interference effects appear. In addition, it is seen that there is an univalued relationship between thickness

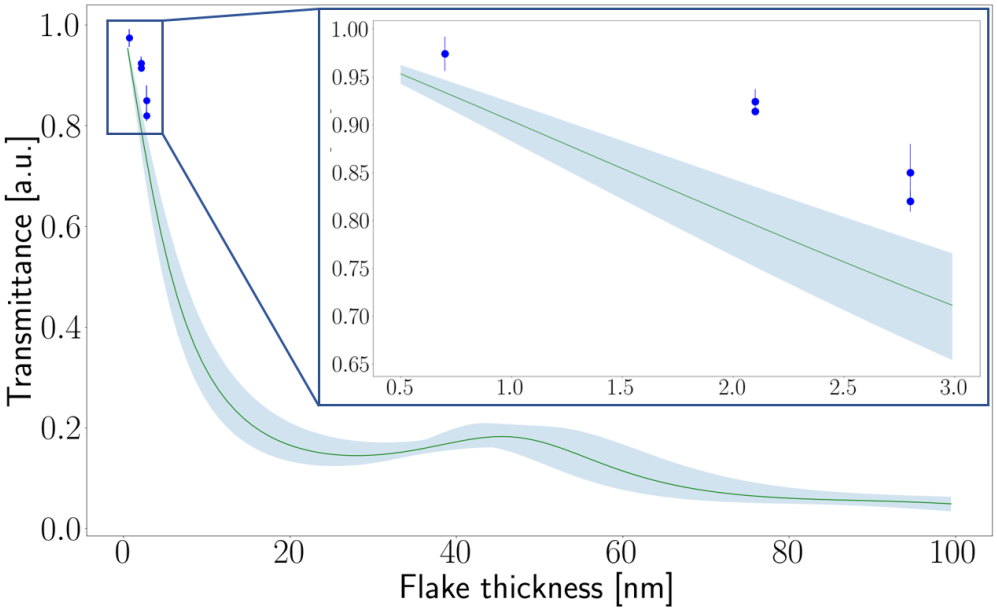

FIGURE 4.2: Comparison between the experimental points (blue) and the numerical calculation (green). The shaded area includes all the possible values of $n + i\kappa$ within a range of $\pm$ 10% of their nominal value.

and transmittance up to 15 nm. This could help researchers to characterize crystals with many layers where Raman scattering does not resolve. Remember that Raman scattering is ineffective from 5 layers onwards. This could represent and advance for the scaled production of thin layers.

5 Electrical measurements in a single layer MoS_2 phototransistor

In this section, I will probe some of the electrical characteristics of a single layer of MoS_2. I will use a device fabricated following the steps of Chapter 1. Firstly, I will explain what is a transistor and a phototransistor, as well as the most important processes that take part in it (mainly photocurrent and photogating). I will show an IV characteristic (Intensity v. Voltage) of the channel. Then, study the difference in the current if the device is receiving light or not, varying the gate voltage. And lastly, show the relationship between the photocurrent and the power of the incident light.

5.1. Field-Effect Transistor

In electronics, a transistor is a device that regulates current or voltage flow and acts as a switch for electronic signals. There are many types of transistor that exploit different physical phenomena and configurations. Most known families are Bipolar Junction transistors (BJT) and Field-Effect Transistors (FET) (Teja, 2021). The latter create an electric field that tunes the density of carriers in the channel (i.e. the material in which the current flows).

There are four main components in a FET: (i) the channel is the zone where the current flow is concentrated; (ii) the source and the drain are the contacts at each side of the channel, between them it is applied a voltage V_{ds}; and the (iii) gate is the element that controls the current I_d by means of a voltage application. This gate voltage V_{gs} is what creates the electrostatic field in the proximity of the insulator (Fig. 5.1.a). That creates a minority carriers transport current from the source to the drain.

Firstly, we are going to study the variation of the resistance at different voltages. A metal-semiconductor junction can behave in two different ways depending on the energy bands levels of both materials. They are ohmic contact and Schottky barrier. Whereas the former is good for conduction and the manipulation of signals in semiconductors, the Schottky barrier creates a rectifying contact. This means that the conduction is biased in one of the polarizations of the device (Neamen, 2012). Moreover, they have great contact resistance. This is what happens near the contacts of our device.

The carriers will have to overpass this barriers in order to contribute to the current generation. At low voltages, only some thermal excitated carriers will be able to cross the barrier, but as the voltage increases the barrier gets

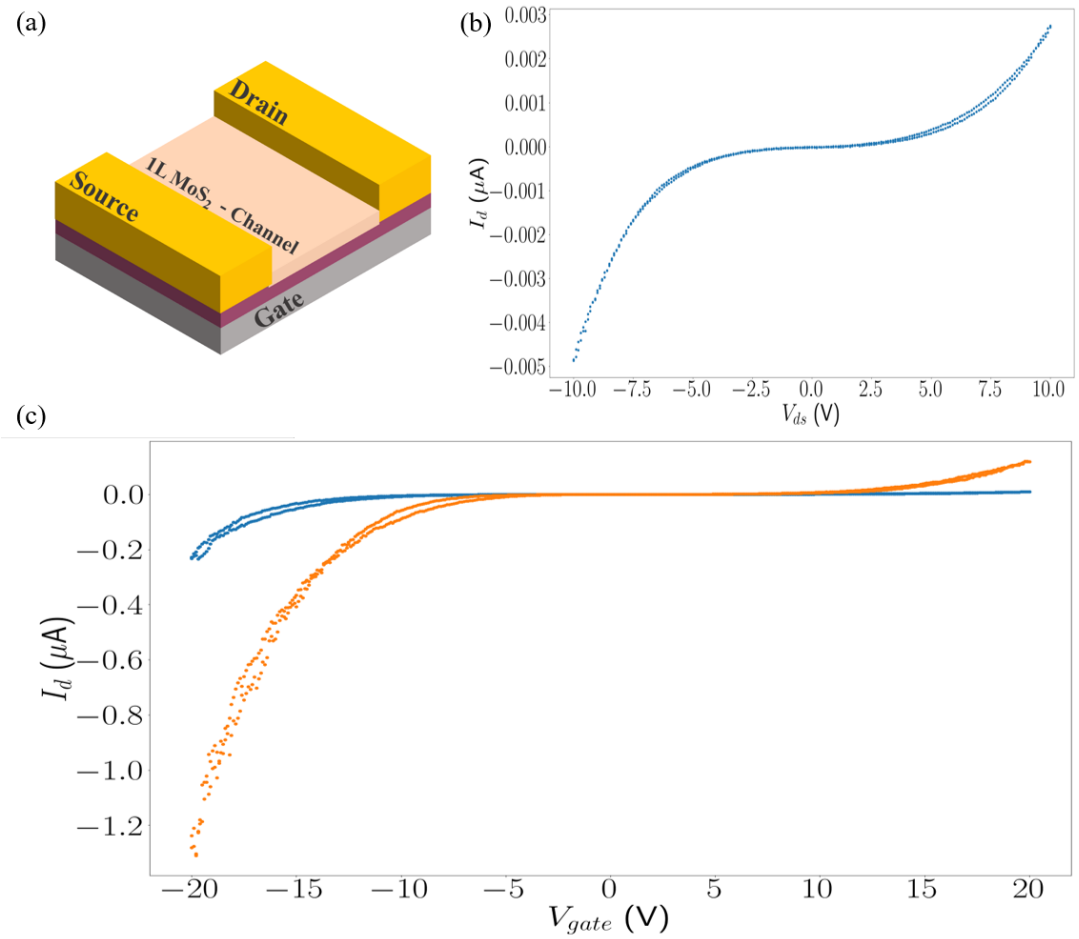

FIGURE 5.1: (a) Schematic view of a transistor. Source and Drain are Ti-Au contacts, and the base of Si is the Gate electrode. (b) IV characteristic of the transistor. (c) Comparison between light on (orange) and off (blue) current flow with $V_{ds} = 2.5V$.

thinner and this allows carriers to *tunnel* to the other side. One can see how the resistance of the device varies at different voltages (Fig. 5.1.b). In each of the polarizations, one of the contacts acts as a Schottky barrier. The barrier height and width highly depends on the contact surface, the carrier density and the local charge states. For that reason, the curve is not symmetric.

5.1.1. Phototransistor. Photocurrent and photogating

A phototransistor exploits the change in the current when light is irradiated in the channel. In this case, the light acts as the gate. The incident photons create electron-hole pairs that contributes to the current. This contribution is defined as the photocurrent. The other effect of interest is the photogating effect. It is a photocurrent generation mechanism that acts even when the illumination has ceased. If the channel has a high density of charge traps, the photogenerated electrons are trapped in the surface oxide and acts as an effective gate (Yamamoto, Ueno, and Tsukagoshi, 2018).

We expose the channel to a laser beam with a fixed V_{ds} and varying V_{gs} to see how the current changes. In figure 5.1.c it is shown how the device conducts more when the light is on. As before, the curves are asymmetric, which is better noted in the *ON* curve.

5.2. Photocurrent dependance on the incoming light power

One can measure the dependence of the current with the illumination power density. The power density P_D is related to the number of incoming photons. The density of absorbed photons can be expressed as $\phi_A = \eta P_D \lambda / hc$, being η the optical absorption of the material (Vaquero et al., n.d.).

The dynamics of photoexcited carriers is analyzed using a modified Hornbeck-Haynes model, assuming the main photocarrier mechanism is Shockley-Read-Hall recombination mediated by midgap states. The trapped charges in this states induce a gain in the current due to photogating effect. The dependence with the power density can be studied with a phenomenological expression such as $I_{PC} \propto P_D^{\alpha}$.

In my case, I changed the power density for 20 seconds, leaving a 20 seconds gap between each illumination, using a different filter. The filters used where of 0.1%, 1%, 3% and 5% of the total laser intensity. In Figure 5.2(a) can be seen how the current increases hugely when the light is switched on. Moreover, each time the ground intensity prior to the illumination is higher. This is due to the trapped charges that act as a gate doping the material. We can see also the relaxation when the light is turned off. Figure 5.2(b) shows the fitting, which is near the theoretical adjustment with $\alpha \approx 0.5$.

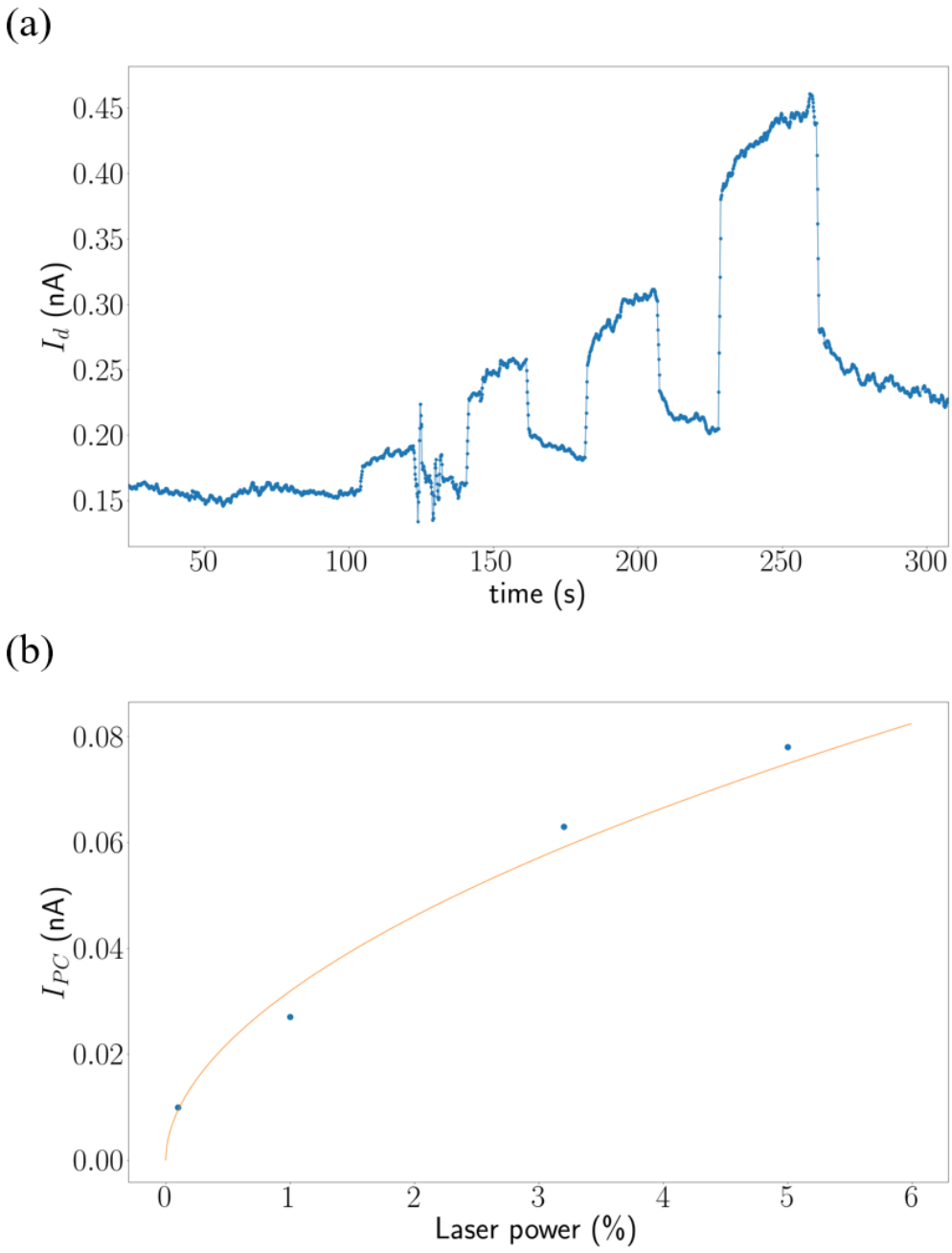

FIGURE 5.2: (a) Current over time applying different laser powers.(b) the points fit to a curve $I_{PC} = kP^{\alpha}$ with $\alpha = 0.53$.

6 Conclusions

Conclusions

In this work, I have exposed the promising characteristics of 2D materials and TMDs and why they are worthy of study at a fundamental and application level. Later on, implemented a method of characterization of MoS_2 flakes which is faster than other methods such as Raman spectroscopy or AFM, designing an algorithm to identify monolayers with the optical microscope. This method is non-invasive and infers no damage to the samples. When comparing to a simple model, the results fit well and reproduce the same behaviour. Moreover, the simulation show that the optical identification method can be extrapolated to thicker flakes. Finally, I probed some optoelectronic characteristics of the material in Chapter 5. The results show the intrinsic semiconductor properties and the rapid photoresponse of MoS_2. Following works could improve the characterization technique, upgrading the transmission setup of the microscope, studying the use of different filters at different wavelengths to get more contrast, and improve the fitting with more samples.

Conclusiones

Tras haber puesto de manifiesto las posibilidades que ofrecen los materiales 2D y en particular los TMDs, queda ampliamente justificada la importancia de su estudio al nivel más fundamental y en el desarrollo de aplicaciones. Se ha probado un método para agilizar la indentificación de monocapas de estos materiales para la fabricación de dispositivos para investigación y se ha mejorado satisfactoriamente el proceso. Este nuevo método es más rápido que la caraterización por espectroscopía Raman o AFM y se puede usar de forma rutinaria. Además, con la propuesta de un modelo numérico básico que reproduce los resultados obtenidos experimentalmente, se infiere que este método de identificación óptica puede funcionar para estructuras con más de 4 y 5 capas, donde el método de espectroscopía Raman ya no resuelve el grosor. En el último capítulo se muestran medidas eléctricas sobre un fototransistor hecho con una monocapa de MoS_2. En ellas se pueden ver desde las propiedades más básicas de este semiconductor hasta la rápida respuesta a estimulaciones luminosas. Las limitaciones que se han observado en la iluminación por transmisión podrían ser solventadas en futuros trabajos cambiando la configuración de la toma de imágenes. Además, el estudio de filtros a diferentes longitudes de onda podría aumentar el contraste de los flakes con el fondo. Finalmente, si se midieran más muestras se podría mejorar la estadística y la y el ajuste.

A Python scripts

A.1. Acquisition of transmittance from an image

```
# -*- coding: utf-8 -*-
"""
Created on Tue Feb  9 16:01:24 2021

Program to calculate the ratio of intensity
through a flake compared to the background.
Write %matplotlib qt in the Terminal before
executing the script.
@author: alean
"""

import numpy as np
import matplotlib.pyplot as plt
from matplotlib import patches
from skimage import io

l = 30 #lado del cuadrado

def tellme(s):
    print(s)
    plt.title(s, fontsize=16)
    plt.draw()

def rectangle(x,y):
    xx= x - l/2
    yy= y - l/2
    ax.add_patch(patches.Rectangle(
        (xx,yy),
        width=l,
        height=l,
        fill=0))

#-----------------------------------------------
#Read the image from the directory
img= io.imread('C://')

#-----------------------------------------------
```

```
#Figure
fig = plt.figure()
ax = fig.add_subplot(1,1,1)
blueimg = img[:,:,1]
plt.imshow(blueimg)
plt.grid()
tellme('MEDIDOR DE TRANSMITANCIA')
plt.waitforbuttonpress()

while True:
    bg = []
    pt = []
    tellme('Seleccione un punto del background')
    bg = np.asarray(plt.ginput(1, timeout=-1))
    rectangle(bg[0,0],bg[0,1])
    print('Background: {}'.format(bg))

    tellme('Seleccione un punto en el centro del flake')
    pt = np.asarray(plt.ginput(1, timeout=-1))
    rectangle(pt[0,0], pt[0,1])
    print('Flake: {}'.format(pt))

    break


#-----------------------------------------------
#Mean value
def meanval(x,y):
    #x and y are permuted in the plot
    mean = np.mean(blueimg[int(y-l/2):int(y+l/2),
    int(x-l/2):int(x+l/2)])
    return mean


ir = meanval(pt[0,0], pt[0,1])/ meanval(bg[0,0], bg[0,1])
print('La transmitancia de esta región es: {}'.format(ir))
```

A.2. Transfer Matrix Method calculation

```
# -*- coding: utf-8 -*-
"""
Created on Tue Mar  9 18:46:02 2021

@author: alean
"""
import numpy as np
import matplotlib.pyplot as plt

#Program that computes the transfer
#matrix through a collection of media
#Media
# 1 --- Air
# 2 --- PDMS
# 3 --- MoS2

#Parameters
ldo = 530 #wavelength (in nm)
#refraction indexes
n1 = 1.0003
n2 = 1.4051 #+ 1.48e-6j #Zhang et al. 2020
n3 = 5.0774 + 0.90802j
#thicknesses
d3 = 0.7 # of a monolayer (in nm)

#Definition of the scattering an propagation matrix
#Scattering matrix such as x_j = S_ij * x_i
#Defined as the pass from i to j
def S(ni,nj):
    SS = np.zeros((2,2), dtype='cfloat')
    t_ji = 2*nj/(ni+nj)
    r_ji = (nj-ni)/(nj+ni)
    SS[0,0]= 1/t_ji
    SS[0,1]= r_ji/t_ji
    SS[1,0]= r_ji/t_ji
    SS[1,1]= 1/t_ji
    return SS

#Propagation matrix through a medium of
#complex refractive index ni + j*ki and thickness d
def P(ni,d):
    PP = np.zeros((2,2), dtype= 'cfloat')
    phi = 2*np.pi*d*ni/ldo
    PP[0,0]= np.exp(-1j * phi)
    PP[1,1]= np.exp(1j * phi)
```

```
    return PP

#Calculus of transmittance of PDMS only
MM = S(n2,n1)
T_PDMS = n2/n1* 1/(abs(MM[0,0]))**2
print('Transmisión PDMS: {}'.format(T_PDMS))

#Calculus of transmittance of 1L
MM = S(n2,n3)
MM = np.matmul(P(n3,d3), MM)
MM = np.matmul(S(n3,n1), MM)
T_1L = n2/n1* 1/(abs(MM[0,0]))**2
print('Transmisión 1L: {}'.format(T_1L))
print('T_1L / T_PDMS: {}'.format(T_1L/T_PDMS))

#Calculus of transmittance for arbitrary thickness
#d of the MoS2 flake
def Transmi(e):
    MM = S(n2,n3)
    MM = np.matmul(P(n3,e), MM)
    MM = np.matmul(S(n3,n1), MM)
    T = n2/n1* 1/(abs(MM[0,0]))**2
    T = T/T_PDMS
    return T

x = np.arange(0.5, 100, 1)
T = []
for i in range(len(x)):
    T.append(Transmi(x[i]))

#Error area (calculated using n and k w/ a variation of 10%)
nn3 = np.ndarray((100,100), dtype='cfloat')
for i in range(100):
    for j in range(100):
        nn3[i,j]= (0.9 + i*0.2/99)*np.real(n3) +
        (0.9 + j*0.2/99)*np.imag(n3)*1j

nn3 = np.ndarray.flatten(nn3)

errTup = []
errTdown = []

for i in range(len(x)):
    Max = 0.
    Min = 1.
    for j in range(len(nn3)):
        n3 = nn3[j]
```

```
        val = Transmi(x[i])
        if val>=Max:
            Max = val
        if val<=Min:
            Min = val
    errTup.append(Max)
    errTdown.append(Min)



#EXPERIMENTAL DATA
Transmit = [0.974,0.924,0.914,0.85,0.820]
yerror = [0.018,0.013,0.002,0.03,0.011]
e = [0.7, 2.1,2.1,2.8, 2.8]

#PLOTTING.....................................................

#title = 'Transmittance coefficient'
fig=plt.figure(figsize=(15,9))
ax = fig.add_subplot(111)
ax.plot(x,T, 'g')
ax.fill_between(x, errTup, errTdown, alpha=0.2)
ax.errorbar(e, Transmit, yerr = yerror, fmt='bo')
plt.rc('text', usetex=True)
plt.gca().set_aspect('auto')
plt.gca()
font = {'style': 'normal',
                    'color': 'black',
                    'weight': 'normal',
                    'size': 64,
                    }
#plt.title(title, fontdict=font)
plt.xticks(fontsize=32)
plt.xlabel('Flake␣thickness␣[nm]', fontdict=font)
#plt.xlim([np.amin(x[0:Nx-1]),np.amax(x[0:Nx-1])])
plt.ylabel('␣Transmittance␣[a.u.]', fontdict=font)
plt.yticks(fontsize=32)
plt.show()
```

Bibliography

Aitken, Hugh G. J. (1979). "Revolution in Miniature: The History and Impact of Semiconductor Electronics. By Ernest Braun and Stuart Macdonald. New York, Cambridge University Press, 1978. Pp. 231. 16.95.". In: *Business History Review* 53.2, pp. 280–283. ISSN: 0007-6805. DOI: 10.2307/3115036. URL: https://www.cambridge.org/core/product/identifier/S000768050003035X/type/journal_article.

Bukharaev, Anastas Akhmetovich et al. (2018). "Straintronics: a new trend in micro-and nanoelectronics and materials science". In: *Physics-Uspekhi* 61.12, p. 1175.

Buscema, Michele et al. (n.d.). *The effect of the substrate on the Raman and photoluminescence emission of atomically thin MoS 2*. Tech. rep.

Castellanos-Gomez, Andres et al. (2014). "Deterministic transfer of two-dimensional materials by all-dry viscoelastic stamping". In: *2D Materials* 1.1, p. 011002.

Choi, Wonbong et al. (2017). "Recent development of two-dimensional transition metal dichalcogenides and their applications". In: *Materials Today* 20.3, pp. 116–130. ISSN: 1369-7021. DOI: https://doi.org/10.1016/j.mattod.2016.10.002. URL: https://www.sciencedirect.com/science/article/pii/S1369702116302917.

Clericò, Vito et al. (2020). "Fabrication and characterization of quantum materials: graphene heterostructures and topological insulators". In.

Das, Saptarshi et al. (2015). "Beyond Graphene: Progress in Novel Two-Dimensional Materials and van der Waals Solids". In: *Annual Review of Materials Research* 45.1, pp. 1–27. ISSN: 1531-7331. DOI: 10.1146/annurev-matsci-070214-021034. URL: http://www.annualreviews.org/doi/10.1146/annurev-matsci-070214-021034.

Feynman, Richard P. (2011). "There's plenty of room at the bottom". In: *Resonance* 16.9, pp. 890–905. ISSN: 09718044. DOI: 10.1007/s12045-011-0109-x. URL: http://calteches.library.caltech.edu/47/2/1960Bottom.pdf..

Geim, A. K. and I. V. Grigorieva (2013). *Van der Waals heterostructures*. DOI: 10.1038/nature12385. arXiv: 1307.6718. URL: https://www.nature.com/articles/nature12385.

Joensen, Per, R. F. Frindt, and S. Roy Morrison (1986). "Single-layer MoS2". In: *Materials Research Bulletin* 21.4, pp. 457–461. ISSN: 00255408. DOI: 10.1016/0025-5408(86)90011-5.

Koppens, F. H.L. et al. (2014). *Photodetectors based on graphene, other two-dimensional materials and hybrid systems*. DOI: 10.1038/nnano.2014.215. URL: www.nature.com/naturenanotechnology.

Landau, Lev Davidovich (1937). "Zur Theorie der phasenumwandlungen II". In: *Phys. Z. Sowjetunion* 11.545, pp. 26–35.

Li, Xiao and Hongwei Zhu (2015). "Two-dimensional MoS2: Properties, preparation, and applications". In: *Journal of Materiomics* 1.1, pp. 33–44. ISSN: 2352-8478. DOI: https://doi.org/10.1016/j.jmat.2015.03.003. URL: https://www.sciencedirect.com/science/article/pii/S2352847815000040.

Mogera, Umesha and Giridhar U. Kulkarni (2020). *A new twist in graphene research: Twisted graphene*. DOI: 10.1016/j.carbon.2019.09.053.

Molybdenum Disulfide (MoS2):Theory Applications (2021). URL: https://www.ossila.com/pages/molybdenum-disulfide-mos2.

Neamen, Donald A (2012). *Semiconductor physics and devices: basic principles*. New York, NY: McGraw-Hill.

Novoselov, K. S. et al. (2004). "Electric field in atomically thin carbon films". In: *Science* 306.5696, pp. 666–669. ISSN: 00368075. DOI: 10.1126/science.1102896. URL: https://science.sciencemag.org/content/306/5696/666https://science.sciencemag.org/content/306/5696/666.abstract.

Taghavi, Najme S. et al. (2019). "Thickness determination of MoS2, MoSe2, WS2 and WSe2 on transparent stamps used for deterministic transfer of 2D materials". In: *Nano Research* 12.7, pp. 1691–1695. ISSN: 19980000. DOI: 10.1007/s12274-019-2424-6. URL: https://doi.org/10.1007/s12274-019-2424-6.

Teja, R. (Apr. 2021). *Types of Transistors - Junction Transistors and FETs*. URL: https://www.electronicshub.org/transistors-classification-and-types/.

Vaquero, Daniel et al. (n.d.). *Photoconductivity regimes in monolayer MoS 2 phototransistors*. Tech. rep.

Vaquero, Daniel et al. (2020). "Excitons, trions and Rydberg states in monolayer MoS2 revealed by low-temperature photocurrent spectroscopy". In: *Communications Physics* 3.1. ISSN: 23993650. DOI: 10.1038/s42005-020-00460-9. URL: http://dx.doi.org/10.1038/s42005-020-00460-9.

Wei, Wei, Ying Dai, and Baibiao Huang (2017). "Straintronics in two-dimensional in-plane heterostructures of transition-metal dichalcogenides". In: *Physical Chemistry Chemical Physics* 19.1, pp. 663–672.

What is Raman Spectroscopy? - HORIBA (n.d.). URL: https://www.horiba.com/en_en/raman-imaging-and-spectroscopy/.

Xu, Xiaodong et al. (2014). "Spin and pseudospins in layered transition metal dichalcogenides". In: *Nature Physics* 10.5, pp. 343–350.

Yamamoto, Mahito, Keiji Ueno, and Kazuhito Tsukagoshi (2018). "Pronounced photogating effect in atomically thin WSe2 with a self-limiting surface oxide layer". In: *Applied Physics Letters* 112.18, p. 181902. ISSN: 00036951. DOI: 10.1063/1.5030525. URL: https://aip.scitation.org/doi/abs/10.1063/1.5030525.

Yin, Zongyou et al. (2012). "Single-layer MoS₂ phototransistors". In: *ACS nano* 6.1, pp. 74–80. arXiv: arXiv:1408.1149.

Zhang, Hui et al. (2015). "Measuring the Refractive Index of Highly Crystalline Monolayer MoS2 with High Confidence". In: *Scientific Reports* 5. ISSN: 20452322. DOI: 10.1038/srep08440.

Zhou, Kai Ge et al. (2014). "Raman modes of MoS2 used as fingerprint of van der Waals interactions in 2-D crystal-based heterostructures". In: *ACS*

Nano 8.10, pp. 9914–9924. ISSN: 1936086X. DOI: 10.1021/nn5042703. URL: www.acsnano.org.